J Biol Inorg Chem (2014) 19:399–414
DOI 10.1007/s00775-013-1085-2

ORIGINAL PAPER

Chitosan-modified cobalt oxide nanoparticles stimulate TNF-α-mediated apoptosis in human leukemic cells

Sourav Chattopadhyay · Sandeep Kumar Dash · Santanu Kar Mahapatra · Satyajit Tripathy · Totan Ghosh · Balaram Das · Debasis Das · Panchanan Pramanik · Somenath Roy

Received: 21 October 2013 / Accepted: 19 December 2013 / Published online: 21 January 2014

Abstract The objective of this study was to develop chitosan-based delivery of cobalt oxide nanoparticles to human leukemic cells and investigate their specific induction of apoptosis. The physicochemical properties of the chitosan-coated cobalt oxide nanoparticles were characterized using transmission electron microscopy, dynamic light scattering, X-ray diffraction, and Fourier transform infrared spectroscopy. The solubility of chitosan-coated cobalt oxide nanoparticles was higher at acidic pH, which helps to release more cobalt ions into the medium. Chitosan-coated cobalt oxide nanoparticles showed good compatibility with normal cells. However, our results showed that exposure of leukemic cells (Jurkat cells) to chitosan-coated cobalt oxide nanoparticles caused an increase in reactive oxygen species generation that was abolished by pretreatment of cells with the reactive oxygen species scavenger *N*-acetyl-L-cysteine. The apoptosis of Jurkat cells was confirmed by flow-cytometric analysis. Induction of TNF-α secretion was observed from stimulation of Jurkat cells with chitosan-coated cobalt oxide nanoparticles. We also tested the role of TNF-α in the induction of Jurkat cell death in the presence of TNF-α and caspase inhibitors. Treatment of leukemic cells with a blocker had a greater effect on cancer cell viability. From our findings, oxidative stress and caspase activation are involved in cancer cell death induced by chitosan-coated cobalt oxide nanoparticles.

Keywords Chitosan · Cobalt oxide · TNF-α · Apoptosis

Introduction

Inorganic metal nanoparticles (NPs) are used extensively as anticancer agents. Recently, cobalt NPs have been used for cancer therapy because cobalt forms organic–metal compounds and metal–biopolymer systems [1] and has a physiological role as a cofactor of vitamin B_{12}. Cobalt-based magnetic fluids have been designed for possible use in medical applications because of their good magnetic properties and their great effects on proton relaxation [2]. Recent development work has largely focused on the use of new metal NPs such as cobalt and nickel NPs. Cobalt NPs have the ability to enter cells very rapidly [1], which has drawn the interest of researchers toward cobalt NPs. But the use of cobalt NPs is restricted because of their toxicity. Recent development work has largely focused on new polymeric or inorganic coatings on magnetite/maghemite NPs [3]. This modification involves the chemical/physical modification of the magnetic NP surface with biocompatible

Electronic supplementary material The online version of this article (doi:10.1007/s00775-013-1085-2) contains supplementary material, which is available to authorized users.

S. Chattopadhyay · S. K. Dash · S. Tripathy · B. Das · S. Roy (✉)
Immunology and Microbiology Laboratory,
Department of Human Physiology with Community Health,
Vidyasagar University,
Midnapore 721102, West Bengal, India
e-mail: roysomenath@hotmail.com

S. Kar Mahapatra
School of Chemical and Biotechnology,
SASTRA University, Thanjavur 613401, Tamil Nadu, India

T. Ghosh · D. Das
Department of Chemistry, University of Calcutta,
92, A.P.C Road, Kolkata 700009, India

P. Pramanik
Nano Materials Laboratory, Department of Chemistry,
Indian Institute of Technology,
Khargapur 721302, West Bengal, India

Table 1 Percentages of propidium iodide (*PI*)-positive Jurkat cells and normal lymphocytes

	Control (%)	CS-CoO NPs (%)		
		50 μg/mL	100 μg/mL	200 μg/mL
Jurkat cells	1.66	25.66	32.25	64.23
Normal	1.83	4.81	13.87	31.45

CS-CoO NPs chitosan-coated colbalt oxide nanoparticles

compounds which offer a promising alternative in the coupling of organic components to metal oxides [4].

Chitosan is a cationic polysaccharide made by alkaline N-deacetylation of chitin. The cationic property of chitosan is exploited in the recovery of proteins from food processing wastes and in the chelation of heavy metals from wastewater [5]. However, chitosan-related applications are limited by the substance's insolubility at neutral or high pH [4]. Therefore, the aim of this work was to demonstrate the feasibility of the combination of chitosan with inorganic NPs as an efficient approach to produce anticancer materials with few adverse effects [5]. It has been reported that chitosan-conjugated metal oxide NPs show better activity toward a microbial population [6]. Combining chitosan with magnetic NPs is an alternative approach to reduce the adverse effects of magnetic NPs [6].

In our previous work, we used *N*-(phosphonomethyl)iminodiacetic acid coated cobalt oxide (CoO) NPs for anticancer therapy in vitro [7]. In this article, we demonstrate the toxicity of chitosan-coated CoO (CS-CoO) NPs toward Jurkat cells and highlight a possible pathway of CS-CoO NP mediated cell (Jurkat) killing activity. Herein, we report the development of a chitosan-based nanocarrier of CoO NPs (CS-CoO) where CoO NPs are homogeneously confined within a biodegradable nanosphere and demonstrate the efficiency of CS-CoO-induced apoptosis of human Jurkat cells. The apoptotic cell death was investigated by propidium iodide (PI) staining and electron microscopy. We provide evidence that CS-CoO NPs induce apoptosis via activation of caspases 3, 8, and 9. The interplay between reactive oxygen species (ROS) and TNF-α, two major signals for apoptosis, was investigated (Table 1).

Materials and methods

Chemicals and reagents

Cobalt chloride ($CoCl_2 \cdot 3H_2O$), chitosan, PI, RNase A, 3-(4,5-dimethyl-2-thiazolyl)-2,5-diphenyl-2*H*-tetrazolium bromide (MTT), rhodamine B (RhB), Histopaque-1077, and caspase 3, caspase 8, and caspase 9 antibodies were procured from Sigma (St. Louis, MO, USA) and eBiosciences, respectively. RPMI 1640 medium, fetal bovine serum (FBS), penicillin, streptomycin, sodium chloride, sodium carbonate, sucrose, Hanks balanced salt solution, and ethylenediaminetetraacetate (EDTA) were purchased from HiMedia (India). Tris(hydroxymethyl)aminomethane hydrochloride, tris(hydroxymethyl)aminomethane buffer, KH_2PO_4, K_2HPO_4, hydrochloric acid, formaldehyde, and alcohol were procured from Merck (Mumbai, India). Commercially available dimethyl sulfoxide was procured from HiMedia (India) and was purified by vacuum distillation over KOH. All other chemicals were from Merck, and were of the highest purity grade available.

Synthesis of CS-CoO NPs

High molecular weight chitosan (more than 75 % deacetylated) was used for the synthesis of CS-CoO NPs. Chitosan solution (1 mg/mL) was prepared in 1 % acetic acid and the mixture was stirred at 45 °C to obtain a homogeneous solution. The chitosan solution (24 mL) was then mixed with 0.1 N sodium hydroxide solution (75 mL), and 100 mM $CoCl_2$ solution (1 mL) was added to the resulting suspension. The change to a blackish appearance indicated the formation of CS-CoO NPs. After it had been allowed to settle, the suspension was washed twice with sterile distilled water and centrifuged at 2,000 rpm for 5 min. The NPs were then separated using a magnet and washed four times with deionized water. The precipitate was directly dried in a vacuum oven at 50 °C for 20 h. The dried sample was sterilized by autoclaving prior to use.

Quantitative determination of chitosan in CS-CoO NPs

The ninhydrin method was used for quantitative analysis of chitosan present in CS-CoO NPs. Ninhydrin reagent was prepared by dissolving ninhydrin (0.5 g) in 2-propanol (30 mL). The resulting solution was mixed with 20 mL of sodium acetate buffer (pH 5.5). A chitosan standard curve ranging from 100 μg/mL to 1 mg/mL was constructed, and this was used to calculate the quantity of chitosan present in CS-CoO NPs. Ninhydrin reagent (1 mL) was added to the test samples (1 mL) and the mixture was boiled for 30 min. The solution was then cooled to 30 °C and diluted with 50 % ethanol (5 mL). The absorbance at 570 nm was measured with an ultraviolet and visible spectrophotometer (UV-1800; Shimadzu, Kyoto, Japan) [6].

Characterization of NPs

X-ray diffraction

The phase formation and crystallographic state of CS-CoO NPs were determined by X-ray diffraction (XRD)

with an Expert Pro X-ray diffractometer (Philips) using Co Kα radiation ($\lambda = 0.178$ nm). Samples were scanned from 20° to 80° in 2θ increments of 0.040° with 2-s counting time. The hydrodynamic size of the CS-CoO NP aggregates was measured with a Brookhaven 90 Plus particle size analyzer [8].

Dynamic light scattering

The size distribution and zeta potential of the chitosan and CS-CoO NPs were determined by dynamic light scattering (DLS; Zetasizer Nano ZS; Malvern Instruments, Malvern, UK) [7].

Transmission electron microscopy and scanning electron microscopy

The particle size and microstructure were studied by high-resolution transmission electron microscopy with a JEOL (Japan) 3010 high-resolution transmission electron microscope operating at 200 kV according to the method of Chattopadhyay et al. [7] with some modifications. In brief, CS-CoO NPs were suspended in deionized water at a concentration of 1 mg/mL, and then the sample was sonicated using a sonicator bath until the sample formed a homogeneous suspension. For size measurement, sonicated stock solution of all CS-CoO NPs (0.5 mg/mL) was diluted 20 times. Transmission electron microscopy and scanning electron microscopy were used to characterize the size and shape of the CS-CoO NPs. A drop of aqueous CS-CoO NP suspension was placed onto a carbon-coated copper grid and this was dried in air to obtain transmission electron microscopy and scanning electron microscopy images.

Fourier transform infrared study

The conjugation of chitosan with CoO NPs was investigated by Fourier transform infrared (FTIR) spectroscopy with a PerkinElmer Spectrum RX I FTIR system according to the method of Ghosh et al. [8] with some modifications. In brief, 1.0 mg sticky mass of CS-CoO NPs with 100 μL KBr medium and a thin film was prepared on a sodium chloride plate by the drop casting method and under atmosphere separately. The FTIR spectra were recorded between 500 and 4,000 cm^{-1}.

Dissolution study

CS-CoO NPs were suspended in medium (without FBS and antibiotics) and incubated for 1 week at 37 °C. After the incubation period, the supernatant was used for the estimation of free cobalt ions in the medium by atomic absorption spectroscopy (AAS) using different concentrations of $CoCl_2 \cdot 6H_2O$ as a standard [9].

In vitro toxicity of CS-CoO NPs toward leukemic cell lines

T-cell lymphoma (Jurkat) was cultivated for in vitro experiments. The cell line was obtained from the National Centre for Cell Science (Pune, India). It was cultured in RPMI 1640 medium supplemented with 10 % FBS, 100 U/mL penicillin, 100 μg/mL streptomycin, and 4 mM L-glutamine under a 5 % CO_2 and 95 % humidified atmosphere at 37 °C. Jurkat, K562, and KG1-A cells (2×10^4 cells per milliliter) were seeded into 96 wells of tissue culture plates containing 180 μL of complete medium and CS-CoO NPs were added to the cells at different concentrations (1, 5, 10 25, 50, 100, and 200 μg/mL), and were incubated for 24 h at 37 °C in a humidified incubator (NBS) maintained with 5 % CO_2. The cell viability was estimated by the MTT assay according to the method in our previous report [7].

In vitro cytotoxicity toward normal cells

The lymphocytes were isolated from heparinized blood samples according to the method of Hudson and Hay [10]. Normal human lymphocytes were divided into six groups. Each group contained six Petri dishes (2×10^4 cells per milliliter in each). The cells of each Petri dish of the control and experimental groups were maintained in RPMI 1640 medium supplemented with 10 % FBS, 50 μg/mL gentamicin, 50 μg/mL penicillin, and 50 μg/mL streptomycin at 37 °C in a 95 % air/5 % CO_2 atmosphere in a CO_2 incubator. CS-CoO NPs were added to the cells at different concentrations (1, 5, 10 25, 50, 100, and 200 μg/mL), and were incubated for 24 h at 37 °C in a humidified incubator (NBS) maintained with 5 % CO_2. The cell viability was estimated by the MTT assay according to the method in our previous report [11].

Hemolysis assay

EDTA-stabilized human blood samples were freshly obtained from healthy subjects according to the Hay protocol. First, 5 mL of blood sample was added to 10 mL of phosphate-buffered saline (PBS), and then red blood cells (RBCs) were isolated from serum by centrifugation at 2,200 rpm for 10 min. The RBCs were further washed five times with 10 mL of PBS solution. The purified blood was diluted to 50 mL with PBS. Prior to NP exposure, the absorption spectrum of the positive control supernatant was checked and used only if the absorbance was in the range from 0.50 to 0.55 optical density units to reduce differences in samples from different donors. RBC incubation with deionized water and with PBS were used as the positive

and negative controls, respectively. Then, 0.2 mL of diluted RBC suspension was added to 0.8 mL of CS-CoO solutions at systematically varied concentrations and mixed gently. The NPs suspended in PBS solutions with different concentrations were prepared immediately before RBC incubation by serial dilution. All the sample tubes were kept in the static condition at room temperature for 3 h. Finally, the mixtures were centrifuged at 10,016*g* for 3 min, and 100 μL of supernatant from all samples was transferred to a 96-well plate. The absorbance of the supernatants at 570 nm was determined by using a microplate reader with the absorbance at 655 nm as a reference [12]. The percent hemolysis of RBCs was calculated using the following formula:

$$\text{Percent of hemolysis} = (\text{sample absorbances negative control absorbance})/(\text{positive control absorbances negative control absorbance}) \times 100.$$

Intracellular uptake

NP uptake by Jurkat cells was studied by fluorescence microscopy methods according to our previous report [11]. After the treatment schedule, 2×10^4 cells were seeded into 35-mm cell culture plates. They were incubated in a humidified incubator maintained with 5 % CO_2 at 37 °C. After 8 h, the cells were washed with incomplete medium and were incubated with 200 μg/mL RhB-tagged CS-CoO for fluorescence microscopy. Then the cells were allowed to adhere to a glass coverslip in 35-mm Petri plates, followed by incubation for 4 h at 37 °C in a humidified incubator maintained with 5 % CO_2. Fluorescence images were acquired with a 488-nm laser for differential interference contrast microscopy and a 543-nm laser for RhB excitation using a phase contrast and fluorescence microscope (model CX41; Olympus Singapore).

Estimation of Co^{2+} uptake in Jurkat cells and lymphocytes after treatment with CS-CoO NPs was estimated by AAS. For AAS, cells were harvested at 50 % confluence (2×10^4 cells) and were then treated with CS-CoO NPs at 200 μg/mL for 2, 4, 6, and 8 h. After the treatment schedule, cells were washed twice with equal volumes of PBS with or without 1 mM EDTA. The cells were resuspended in 6 M nitric acid and incubated at 95 °C for 24 h. Acid-digested samples were then assayed for Co^{2+} content with a Shimadzu AA-7000 atomic absorption spectrophotometer. A standard curve of six standard samples (10^{-6}–0.1 M) was prepared using $CoCl_2{\cdot}6H_2O$ salt, dissolved in RPMI 1640 medium. The final cellular Co^{2+} contents before and after treatment with CS-CoO NPs were estimated from the standard curve. The Co^{2+} contents of all buffers and culture medium were normalized to obtain the actual Co^{2+} content of the cells [13].

Measurement of ROS

The production of intracellular ROS was measured using 2,7-dichlorofluorescein diacetate ($DCFH_2$-DA) [14]. The $DCFH_2$-DA passively enters the cell, where it reacts with ROS to form the highly fluorescent compound 2,7-dichlorofluorescein. Briefly, 10 mM $DCFH_2$-DA stock solution (in methanol) was diluted in culture medium without serum or other additives to yield a 100 μM working solution. At the end of exposure with both NPs, cells were washed twice with PBS. Then, cells were incubated in 1.5 mL working solution of $DCFH_2$-DA at 37 °C for 30 min. Cells were lysed in alkaline solution and centrifuged at 2,300*g*. One milliliter of supernatant was transferred to a cuvette, and fluorescence was measured at 520 nm with a fluorescence spectrophotometer (Hitachi F-1700) using 485-nm excitation. The values were expressed as percent fluorescence intensity relative to control wells. Fluorescence micrographs were also taken by phase contrast microscopy.

Pretreatment with *N*-acetyl-L-cysteine

To determine the role of ROS in NP-induced cell death, Jurkat cells was seeded in a 96-well plate at 0.2 mL per well at a concentration of 5×10^5 cells per milliliter. A stock solution of *N*-acetyl-L-cysteine (NAC; Sigma-Aldrich) was made with sterile water and added to cells at 5 and 10 mM for 1 h [14]. After NAC pretreatment, cells were cultured with CS-CoO NPs for 24 h. Viability was determined by the MTT method.

Cellular apoptosis analysis by flow cytometry using PI

To investigate whether CS-CoO NPs are associated with the induction of cellular apoptosis, cells (2×10^4/mL) were treated with 50, 100, and 200 μg/mL CS-CoO NPs for 24 h. After the treatment schedule, the cells were isolated and a homogeneous suspension was prepared in 50 mM PBS and fixed in 70 % ethanol for 1 h on ice. Fixed cells were treated with Triton X and washed with PBS three times. Then, cells were treated with RNase (50 μmol/L) for 30 min at room temperature. After they had been washed with PBS three times, cells were stained with PI (5 μg/mL) solution for 30 min at room temperature. Then, cells were analyzed with a BD Biosciences FACSCalibur flow cytometer. Population distributions were detected by plotting the fluorescence against the forward scattering using the first excitation option. About 10,000 events per sample were acquired. The raw data

obtained from flow cytometry were then subjected to analysis with the computer program Cell Quest [15].

Cytokine analysis

To investigate the effect of CS-CoO NPs on cytokine production, an ELISA was used for determination of TNF-α and IL-10 production. Jurkat cells were cultured at 1×10^5 cells per milliliter and treated with various concentrations of CS-CoO for 24 h. After NP treatment, cell-free supernatants were harvested via successive 10-min centrifugations (2,000, 7,000, and 13,000 rpm) and stored at −80 °C until analysis. ELISA was performed with a BD Biosciences kit, with all samples analyzed in triplicate. Lipopolysaccharide-treated cells were used as a positive control.

Incubation with anti-caspase 3, anti-caspase 8, and anti-caspase 9 antibodies

Cancer cells were cultured with NPs and anti-caspase 3, anti-caspase 8, and anti-caspase 9 antibodies at 1:1,000 dilution for 24 h in RPMI 1640 medium [16, 17]. After incubation, cells were separated and viability was assessed by the colorimetric assay as described by using MTT.

Incubation with pentoxifylline

Pentoxifylline is a xanthine which has been used clinically for the treatment of vascular diseases since 1984 [18–21]. Cancer cells were cultured with NPs and pentoxifylline at a concentration of 2 mM for 24 h in RPMI 1640 medium [22]. After incubation, cells were separated and cytotoxicity was assessed by the colorimetric assay as described by using MTT.

Protein estimation

Protein was determined using bovine serum albumin as a standard, according to the method of Lowry et al. [23].

Statistical analysis

The data were expressed as the mean ± the standard error of the mean ($n = 6$). Comparisons between the means of control and treated groups were made by one-way analysis of variance (using a statistical package; Origin 6.1, OriginLab, Northampton, MA, USA) with multiple-comparison t tests, with $p < 0.05$ as the limit of significance.

Result and discussion

Magnetic NPs with a suitable surface coating show enhanced performance in biomedical applications compared with magnetic NPs without such a coating [24]. One important approach is to modify the surface by coating it with a nontoxic material such as chitosan [25]. We prepared CS-CoO NPs by a coprecipitation method.

Characterization of NPs

X-ray diffraction

The crystal structure of synthesized CS-CoO NPs was determined by XRD. The diffractogram is shown in Fig. 1a. The characteristic peaks at $2\theta = 22.080°$, 36.490°, 43.200°, 52.600°, 70.190°, and 77.500° for CoO NPs, which are marked, respectively, by their indices (111), (220), (311), (400), (511), and (440) in agreement with JCPDS card no. 73-1701, appeared for both bare CoO NPs and CS-CoO NPs. The XRD results revealed the presence of the CoO crystals in the synthesized NPs.

Dynamic light scattering

The measurement of the hydrodynamic size of CS-CoO NPs in PBS by dynamic light scattering shows stable nonaggregated particles with a mean diameter of 80 ± 10 nm (Fig. 1b). The calculated size distribution histogram confirmed the size distribution of NPs (Fig. 1b). These NPs showed good stability in water.

Transmission electron microscopy and scanning electron microscopy

The transmission electron microscopy and scanning electron microscopy morphology of CS-CoO NPs shows nearly spherical geometry with a mean size of 62 ± 6 nm. The result is represented in Fig. 1c and d. The observed size of the NPs was approximately larger than the hydrodynamic diameter obtained from the DLS experiment. Transmission electron microscopy measured the size in the dried state of the sample, whereas DLS measured the size in the hydrated state of the sample, so the size measured by DLS was a hydrodynamic diameter and was larger. However, one has to bear in mind that by transmission electron microscopy we image single particles, whereas DLS gives an average size estimation, which is biased toward the larger-size end of the population distribution. The size of the nanocomplex plays an important role in the delivery of anticancer agents, as NPs up to approximately 400 nm can easily extravasate through the defective vasculature system in tumor tissues and subsequently accumulate in the tumor microenvironment in the presence of ineffective lymphatic clearance [26]. This process is known as the "enhanced permeability and retention" effect and forms the basis of

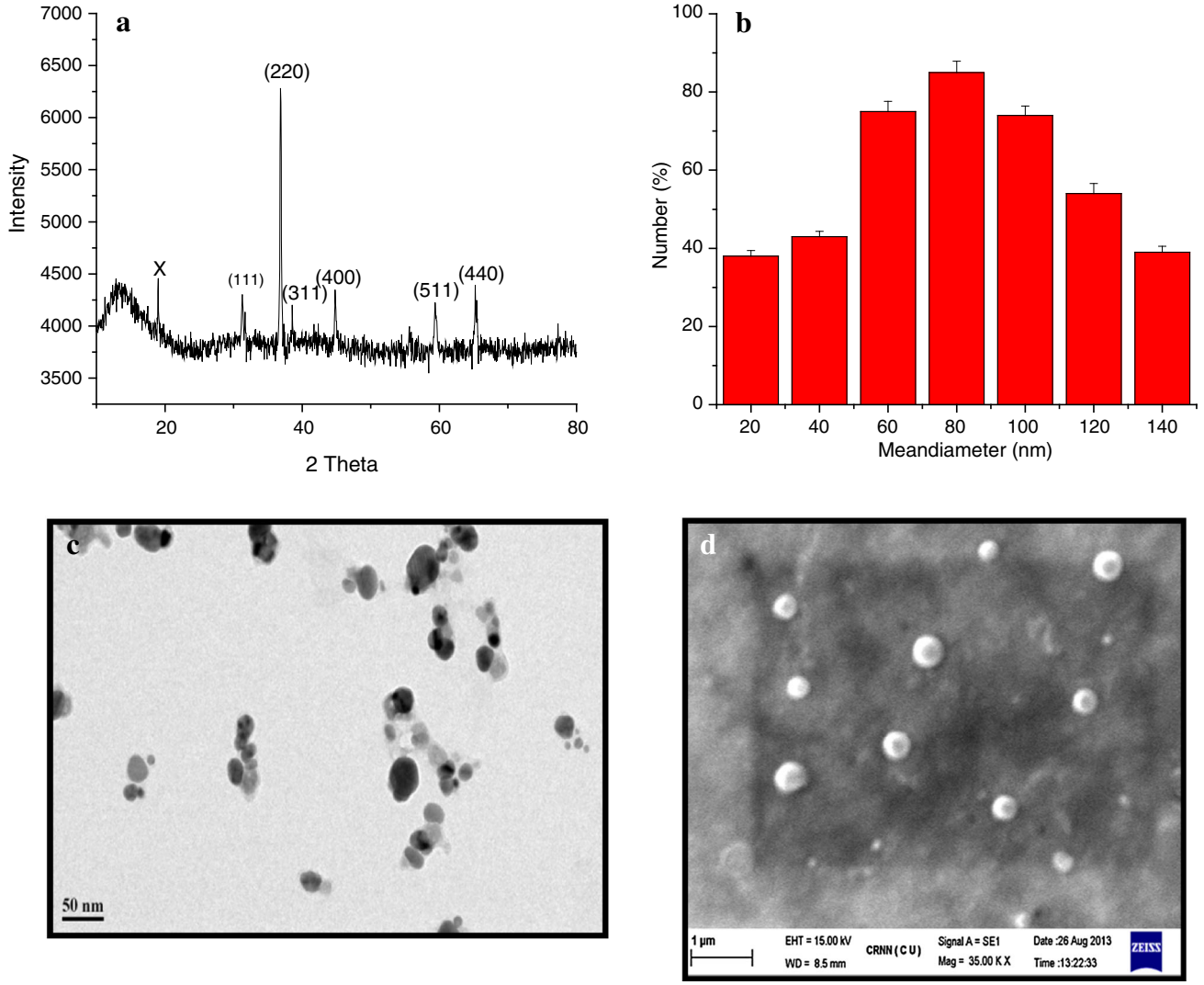

Fig. 1 **a** X-ray diffraction of chitosan-coated cobalt oxide nanoparticles (CS-CoO NPs); *X* denotes the peak of chitosan. **b** Dynamic light scattering of CS-CoO NPs [$n = 6$; values are expressed as the mean ± the standard error of the mean (SEM)]. An *asterisk* indicates a significant difference as compared with the control group. **c** Transmission electron microscopy of CS-CoO NPs. **d** Scanning electron microscopy of CS-CoO NPs

"passive targeting" for in vivo delivery of anticancer drugs encapsulated in polymeric nanocarriers. The CS-CoO NPs prepared in the present study, hence, meet the size limit to be exploited as a drug delivery system. Recently, Sanpui et al. [27] used chitosan-coated silver nanoparticles as a potential anticancer agent.

FTIR study

Conjugation of chitosan with CoO NPs was investigated by FTIR spectroscopy. The FTIR spectra of pure CoO NPs, chitosan, and CS-CoO NPs are shown in Fig. 2. The FTIR spectra show the characteristic infrared band of CoO at 570 cm^{-1}, which indicates the presence of Co–O vibration, and a broad band around. The peaks around 1,615 ± 15 cm^{-1}, assigned to the NH_2 group scissoring, are present in the spectra of both chitosan and CS-CoO NPs, proving that CoO NPs were successfully coated with chitosan polymer on the NP surface. In the FTIR spectrum of chitosan (Fig. 2b), the band at 1,628 cm^{-1} is assigned to NH_2 group scissoring and the peak at 1,156 cm^{-1} is assigned to C–N stretching. In the spectrum of CS-CoO NPs (Fig. 2c), there are peaks at 1,452 and 1,612 cm^{-1}. The results indicated that CoO NPs were successfully coated with chitosan.

Chitosan release

The amount of chitosan leached from the CS-CoO NPs was determined by the ninhydrin method. The amount of

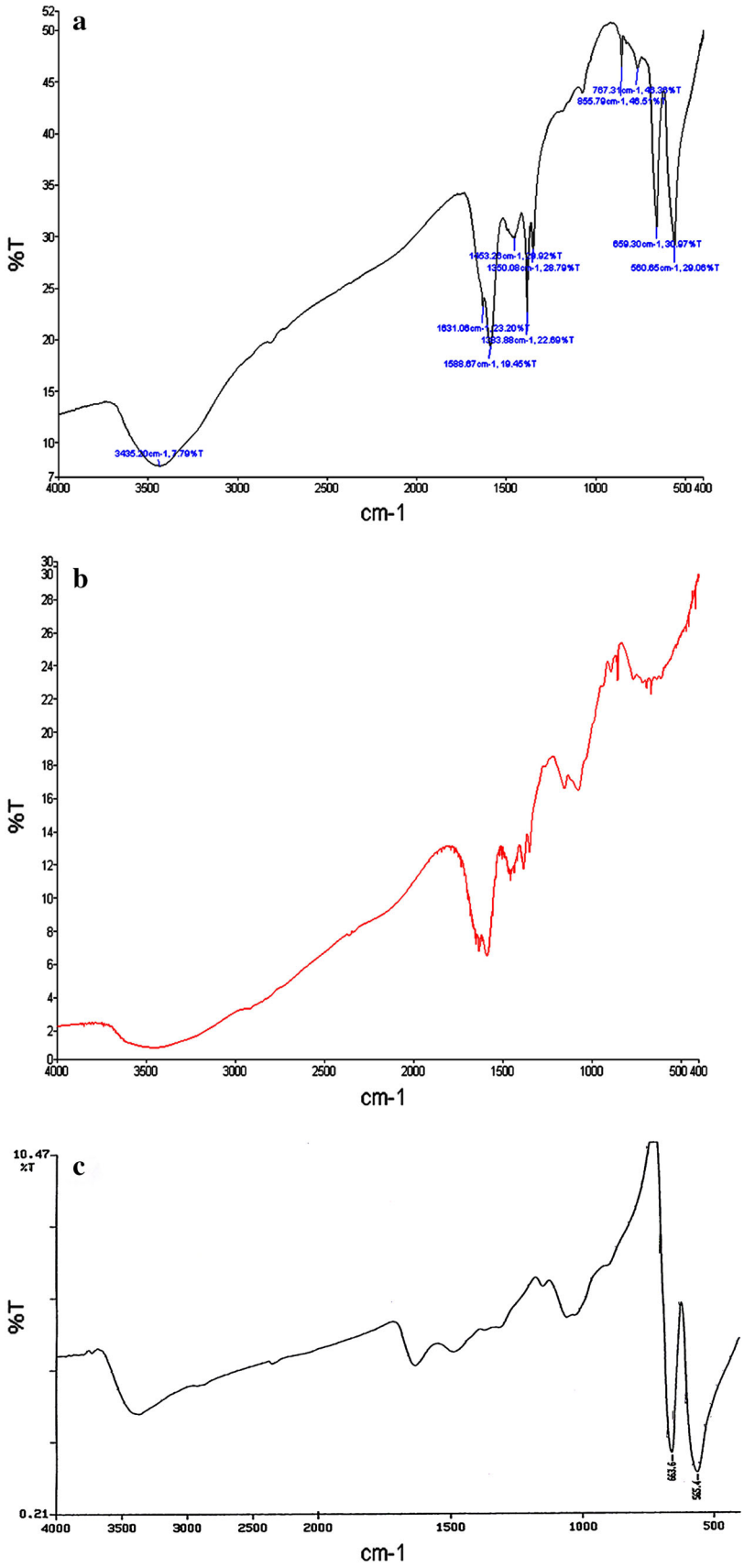

Fig. 2 Fourier transform infrared spectra of pure cobalt oxide nanoparticles (**a**), chitosan (**b**), and CS-CoO NPs (**c**)

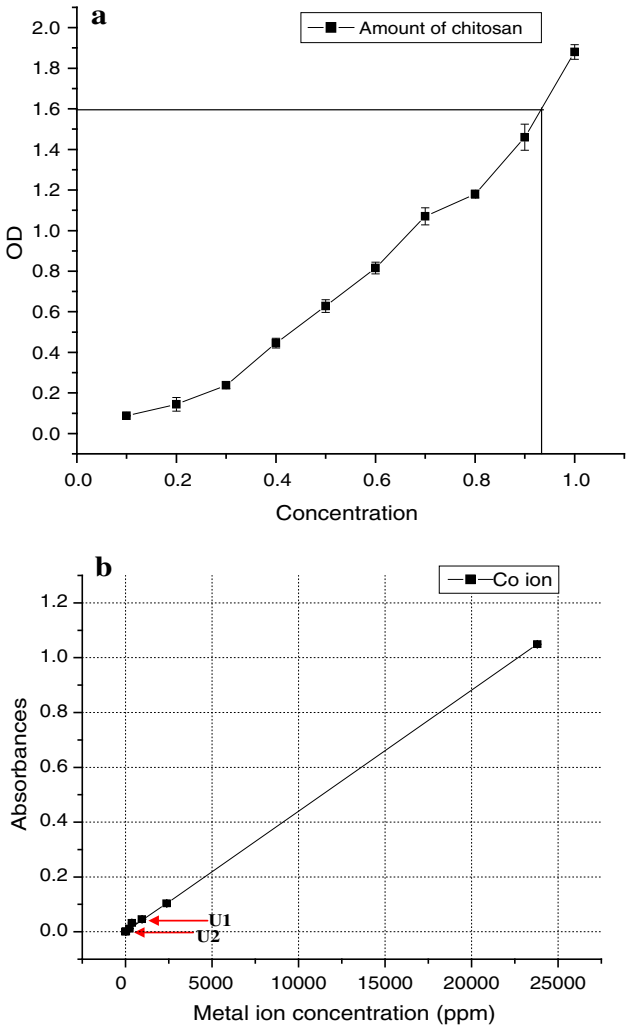

Fig. 3 **a** CS-CoO NPs after 4 days of incubation ($n = 6$; values are expressed as the mean ± SEM). An *asterisk* indicates a significant difference as compared with the control group. **b** Cobalt ion release was measured by atomic absorption spectroscopy; *U1* denotes cobalt ion release from bare cobalt oxide nanoparticles and *U2* denotes cobalt ion release from CS-CoO NPs. *OD* optical density

chitosan present in the medium was 912.44 μg/mL (Fig. 3a).

Cobalt ion release assay

The release of cobalt ions was estimated by AAS. Our results show CS-CoO NPs release much lower concentrations of cobalt ions into a medium of pH 7.0 compared with the control. The cobalt ion release from CS-CoO NPs was greater in acidic solutions (Fig. 3b). The legend modulates the characteristics of the release of free ions from NPs in physiological solutions. To study the effect of decomposition- and complication-induced metal release, the metal ions released from the NP colloid with legends were investigated depending on the legend [28]. We found that lower release of cobalt ions at physiological pH reduces the toxicity of CS-CoO NPs toward normal cells. On the other hand, increased release of cobalt ions at acidic pH influences the cancer cell toxicity of CS-CoO NPs.

In vitro toxicity of CS-CoO NPs toward leukemic cells

CS-CoO NPs exhibit toxicity toward the three cell lines (Jurkat, K562, and KG1-A) tested, but the most promising activity was noted toward Jurkat cells (Fig. S1). So, all further experiments were conducted using Jurkat cells only. CS-CoO NPs exhibit toxicity toward the Jurkat cell line in a dose-dependent fashion. It was observed from our experiment that NPs kill Jurkat cells in proportions of 3.66, 7.25, 15.16, 21.81, 28.84, and 46.84 %, respectively, at doses of 1, 5, 10, 25, 50, and 100 μg/mL. But CS-CoO NPs at a dose of 200 μg/mL kill Jurkat cells significantly ($p < 0.05$), in a proportion of 67.58 % (Fig. 4a). We calculated the half-maximal inhibitory concentration of CS-CoO NPs with regard to Jurkat cells to be 138.16 μg/mL. The present findings demonstrate that Jurkat cells are markedly more susceptible to CS-CoO NPs. The solubility of chitosan at lower pH influences the release of cobalt ions in a cancerous environment and those cobalt ions were toxic to cancer cells. Our results very much correlate with the results of the dissolution study.

In vitro toxicity studies on normal lymphocytes

The toxicity of the CS-CoO NPs was seen in primary human blood lymphocytes purified by density gradient centrifugation, and evaluation of the toxicity profile was conducted by means of the MTT assay (Fig. 4b). It was found that CS-CoO NPs have no or low cytotoxic affects up to 50 μg/mL, but CS-CoO NPs kill normal cells in proportions of 27.87 and 53.45 % at 100 and 200 μg/mL, respectively. The half-maximal inhibitory concentration of CS-CoO NPs was 186.45 μg/mL. Hence, a dose of 100 μg/mL surface-modified NPs is used for biomedical applications. In this study we examined the dose-dependent toxicity profiles of CS-CoO NPs with regard to human primary immune cells. The cellular response is dynamic and the ultimate phenotype is affected by a myriad of competing or overlapping signals present in the microenvironment. Studies were performed to determine how CS-CoO NPs affect normal cells. We found that CS-CoO NPs have much less effect on normal cells than on cancer cells up to 100 μg/mL (Fig. 4b). The toxicity of the CS-CoO NPs depends on the release of cobalt ions from the nanocomplex. Chitosan is insoluble at the physiological pH maintained by normal cells and this was proved by dissolution studies, which also reflect the release of a greater

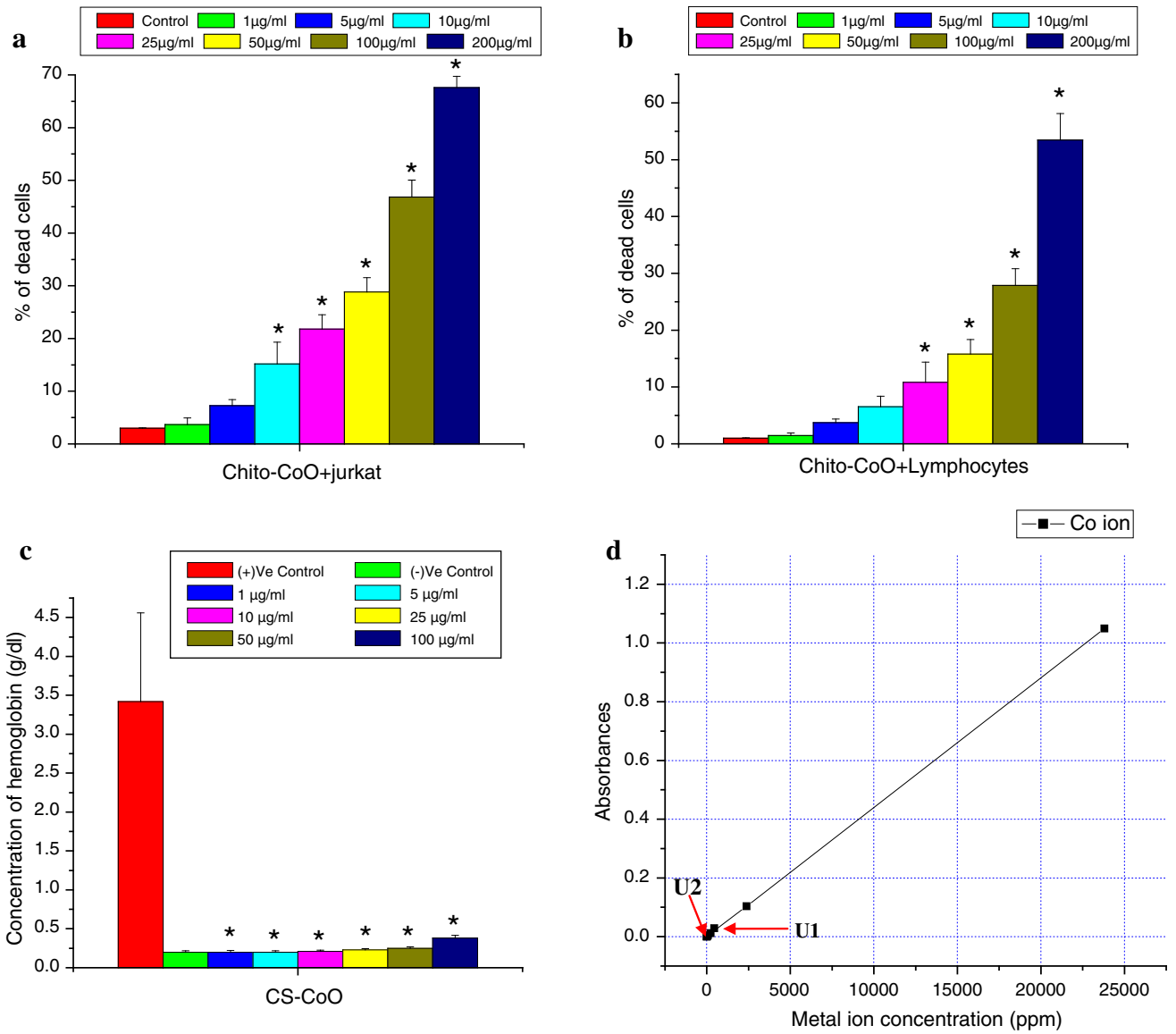

Fig. 4 **a** Cytotoxicity of CS-CoO NPs toward Jurkat cells and **b** cytotoxicity of CS-CoO NPs toward normal human lymphocytes ($n = 6$; values are expressed as mean ± SEM). An *asterisk* indicates a significant difference as compared with the control group. The half-maximal inhibitory concentrations of CS-CoO NPs with regard to Jurkat cells was calculated using the computer program Statistica. **c** Hemolytic activity of CS-CoO NPs is represented as a percentage of the amount of released hemoglobin. **d** The cobalt ion concentration in cancer cell supernatant (*U1*) and normal medium (*U2*) was measured by atomic absorption spectroscopy. *Chito-CoO* chitosan-coated cobalt oxide nanoparticles, *CS-CoO* chitosan-coated cobalt oxide nanoparticles

amount of cobalt ions in medium with the acidic pH maintained by the cancer microenvironment. Moreover, our results show that CS-CoO NPs encourage cytotoxicity at lower pH by releasing cobalt ions.

Dose-dependent hemolytic activity of CS-CoONPs

The hemolysis assay was used to evaluate the cytotoxic effect of CS-CoO NPs on human RBCs. The RBCs were exposed to surface-modified NPs at a range of concentrations from 1 to 100 µg/mL for 3 h. The highest doses used in this work were chosen to model doses often used for in vivo biodistribution, imaging, and therapeutic experiments. As shown in Fig. 4c, the hemolysis of RBCs increases in a dose-dependent manner. The release of hemoglobin in dependent on the concentration of the NPs.

Cobalt ion release assay by AAS

We analyzed the supernatant after centrifugation of 100 µg/mL NPs incubated in normal and cancer cell cultures, and supernatant was collected for cobalt ion

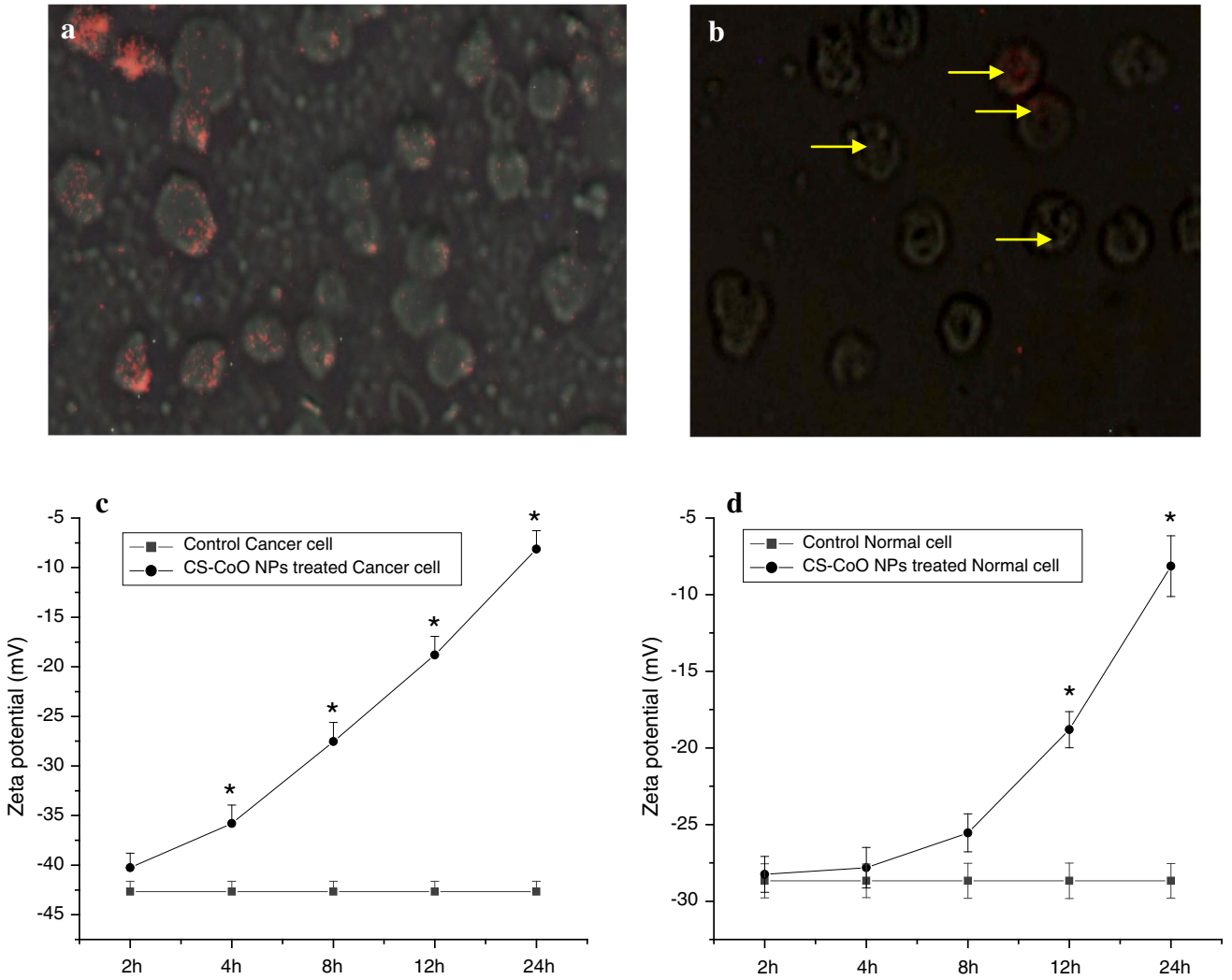

Fig. 5 Fluorescence microscopy shows the intracellular uptake of CS-CoO NPs into Jurkat cells (**a**) and normal cells (**b**). The change of the zeta potential of cancer cells and normal cells before (**c**) and after (**d**) treatment with nanoparticles is shown ($n = 6$; values are expressed as the mean ± SEM). An *asterisk* indicates a significant difference as compared with the control group

concentration assay. Figure 4d shows the concentration of cobalt ions released from CS-CoO NPs. The results show that the CS-CoO NPs release a higher concentration of cobalt ions (45.23 ppm) in cancer cell supernatant than in normal cell supernatant (26.54 ppm). This means that CS-CoO NPs have greater dissolution ability at acidic pH than at normal pH.

Intracellular uptake of NPs

NPs binding to the plasma membrane and cellular uptake are probably a necessary condition for the exertion of cytotoxicity. We have shown by fluorescence microscopy that RhB-tagged CS-CoO NPs were taken up byJurkat cells in in vitro cultures (Fig. 5). Co^{2+} ion uptake was estimated by AAS. It was found that in Jurkat cells Co^{2+} ion uptake was significantly elevated by 0.251 and 0.48 pg Co^{2+} ions per cell at a dose of 200 μg/mL at 6 and 8 h. On the other hand, no significant elevation of Co^{2+} ion uptake was noted in lymphocytes after 8 h (0.23 pg Co^{2+} ions per cell) (Fig. S2). Surface oxidation on contact with cell culture medium or proteins in the cytoplasm liberates Co^{2+} ions from cobalt-based NPs that could amplify the toxicity [29], whereas in CS-CoO NPs, the liberation of ions is less. The fluorescence images (Fig. 5a, b) show the distribution of the CS-CoO NPs in the cytoplasm, leaving the clear zone of the nucleus, indicating cellular uptake instead of adherence to the surface, and the NPs preferentially targeted cancer cells and were internalized. This internalization might be due to endocytosis [30, 31]. The toxicity of CS-CoO NPs toward Jurkat cells depends on the endocytosis of CS-CoO NPs into the cells. Dysregulated

cholesterol metabolism (cholesterol is a part of the cell membranes responsible for plasma membrane integrity, and regulates the uptake process) in leukemic cells [32] may enhance the uptake of CS-CoO NPs into cancer cells. The higher internalization of the CS-CoO NPs was confirmed by the AAS study mentioned previously. In addition, tumor cell membranes contain a higher amount of phospholipids than normal cells [33, 34]. The presence of a high amount of phospholipids may influence the attachment of CS-CoO NPs to the cancer cell membrane, or the acids present in phospholipids may help to attach the CS-CoO nanocomplex and release the free cobalt ions which entered the cell and allow apoptosis by activation of different biochemical processes.

It is established that leukemic cells bear more negative charge on the cell membrane than normal lymphocytes. The positively charged CS-CoO NPs were internalized more into cancer cells than into normal cells. The negative–positive interaction happened between the cancer cell membrane and CS-CoO NPs. The zeta potential change between normal cells and cancer cells could explain the mechanism of uptake of NPs. The cell membrane is overall negatively charged [35] and the loss of negatively charged cell membrane during internalization of positively charged NPs loaded inside the vesicles will cause the zeta potential to become less negative. We found that the binding of charged NPs to the cell-surface plasma membrane will change the zeta potential of the cells (Fig. 5c, d). The binding of positively charged NPs on cell-surface anionic sites may be a useful tool for the investigation of NP-mediated cancer cell toxicity.

CS-CoO NPs induced ROS generation

The potential of CS-CoO NPs to induce oxidative stress was assessed by measuring the ROS. Figure 6 shows that the CS-CoO NPs significantly induced the intracellular production of ROS ($p < 0.05$) in cancer cells. NPs induced 1.82-fold and 2.14-fold increases in ROS production in Jurkat cells at 50, 100, and 200 μg/mL, respectively, from the control level (Fig. 6a, b). A number of studies indicate that certain nanomaterials, including metal oxide NPs, have the potential to cause spontaneous ROS production based on the material composition and surface characteristics, whereas other nanomaterials trigger ROS production only in the presence of select cell systems [36–38]. As there is increasing evidence that ROS at elevated levels act as critical signaling molecules in the induction of apoptosis induced by many different stimuli [39, 40], studies were performed to determine if an NP-induced cytotoxicity occurs via an apoptotic pathway. The results presented in Fig. 6 provide strong evidence that CS-CoO NPs induce apoptosis in cancer cells with the production of ROS. Collectively, these studies indicate that the primary mechanism of cytotoxicity induced by CS-CoO NPs may proceed by CS-CoO NPs inducing the generation of ROS, which then underlies the induction of apoptosis.

Role of NAC in NP-mediated cytotoxicity

Experiments were performed to determine if the cancer cell death that results from NP exposure is dependent on the generation of intracellular ROS. Jurkat cells were exposed to increasing concentrations of the ROS quencher NAC [41, 42] prior to treatment with NPs for 24 h. Figure 6c shows that NAC has significant effects in preventing NP-induced cytotoxicity, with rescue being observed at different concentrations of NP tested. Significant differences ($p < 0.05$) were observed between cultures not pretreated with NAC and pretreated with NAC (5 and 10 mM) for each NP concentration tested. For example, with 10 mM NAC, nearly 100 % viability was retained even at an NP concentration previously shown to reduce cell viability below 10 %. These results indicate that ROS generation plays a causal role in NP-induced cytotoxicity. Apoptosis is prevented by the addition of the ROS quencher at doses of 5 and 10 mM. These observations provide the basis for NP-mediated apoptosis. Development of free radicals is directly responsible for DNA strand breaks or disruption of DNA [43].

Cellular apoptosis analysis by flow cytometry using PI

To confirm CS-CoO NPs mediated cellular apoptosis, a flow-cytometric assay was conducted. After the treatment schedule, Jurkat cells were analyzed with a fluorescence-activated cell sorter using PI. CS-CoO NPs induced cellular apoptosis in Jurkat cells in proportions of 32.25 and 64.23 % (Fig. 7, panels a–d). Cytotoxicity of CS-CoO NPs was evaluated by measuring the cellular uptake of PI (Sigma-Aldrich) after treatment of cells with CS-CoO NPs at different concentrations for 24 h. Normally live cells are impermeable to PI, and PI uptake was used to quantify the population of cells in which membrane integrity was lost. Quantification of cell death was performed by fluorescence-activated cell sorting. Jurkat cells treated with CS-CoO NPs took up PI in a concentration-dependent manner. There was a gradual increase in the number of cells taking up PI with increasing concentration of CS-CoO NPs. The gradual induction of cell death increases several fold beyond a CS-CoO NP concentration of 100 μg/mL with increase in concentration. The PI uptake of normal lymphocytes treated with CS-CoO NPs was minimum up to 100 μg/mL (Fig. 7, panels e–h). The results indicate that cytotoxicity induced by CS-CoO NPs depends on the release of entrapped ions. Acidic conditions help to dissolve the outermost chitosan layer of CS-CoO NPs and help to release cobalt ions and produce cytotoxic agents such as ROS.

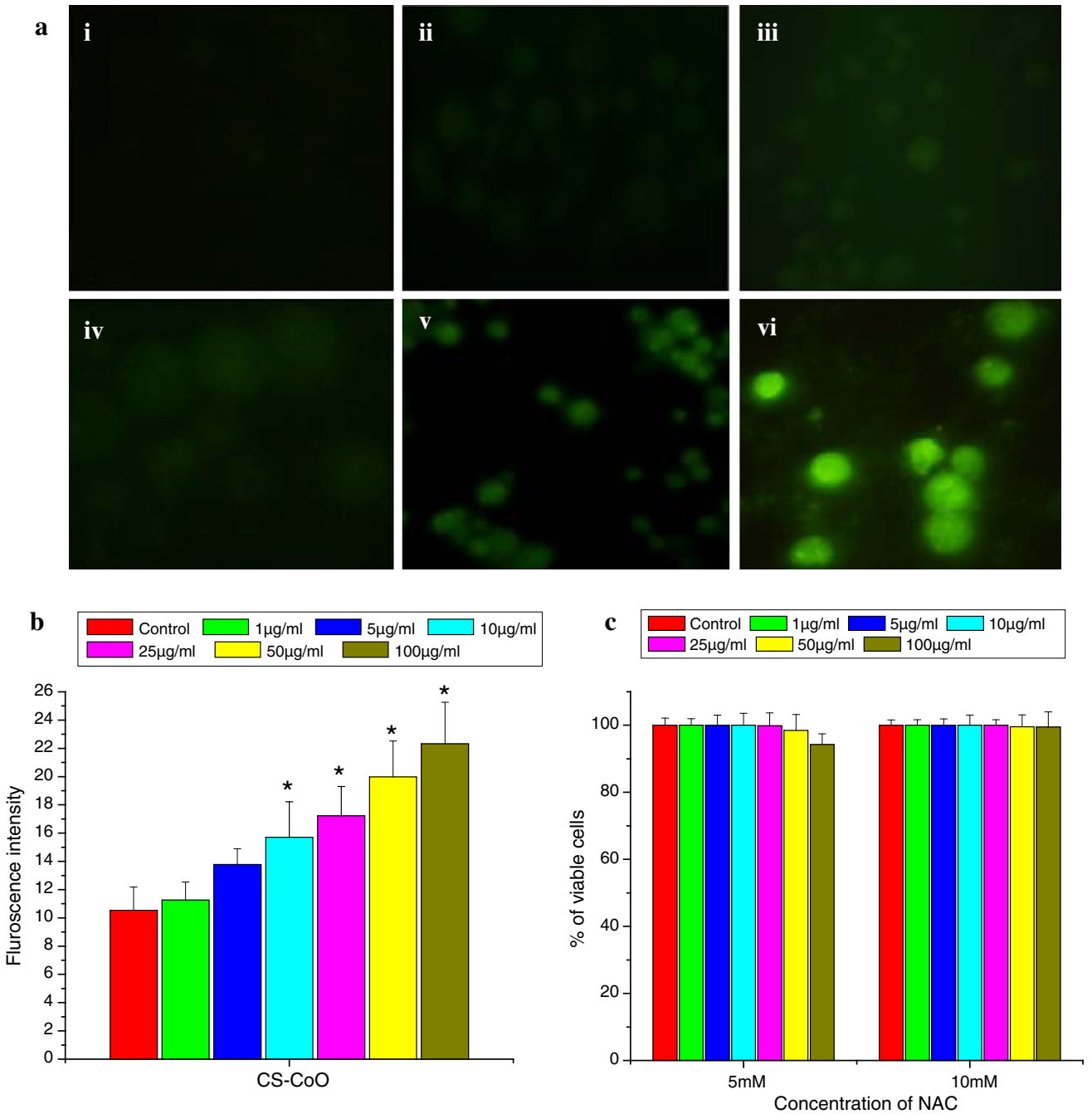

Fig. 6 **a** Fluorescence micrographs of Jurkat cells stained with 2,7-dichlorofluorescein diacetate ($DCFH_2$-DA): *i* Jurkat cell control; *ii* Jurkat cells plus 10 μg/mL CS-CoO NPs; *iii* Jurkat cells plus 25 μg/mL CS-CoO NPs; *iv* Jurkat cells plus 50 μg/mL CS-CoO NPs; *v* Jurkat cells plus 100 μg/mL CS-CoO NPs; *vi* Jurkat cells plus 200 μg/mL CS-CoO NPs. **b** Fluorescence intensity of $DCFH_2$-DA-stained Jurkat cells measured by spectrofluorimetry, and **c** cytotoxicity of CS-CoO NPs toward Jurkat cells with *N*-acetyl-L-cysteine (*NAC*) pretreatment at concentrations of 5 and 10 mM ($n = 6$; values are expressed as the mean ± SEM). An *asterisk* indicates a significant difference as compared with the control group

Cytokine analysis

After the treatment schedule, cell-free supernatants were used to quantify cytokine levels using an ELISA. The results demonstrate significant dose-dependent increases in the level of TNF-α at all NP concentrations tested (Fig. 8a). The results showed that Jurkat cells produce high levels of TNF-α. However, since exposure to particles induced TNF-α level increases of 2.24-fold and 2.86-fold in Jurkat cells at 50 and 100 μg/mL CS-CoO NPs

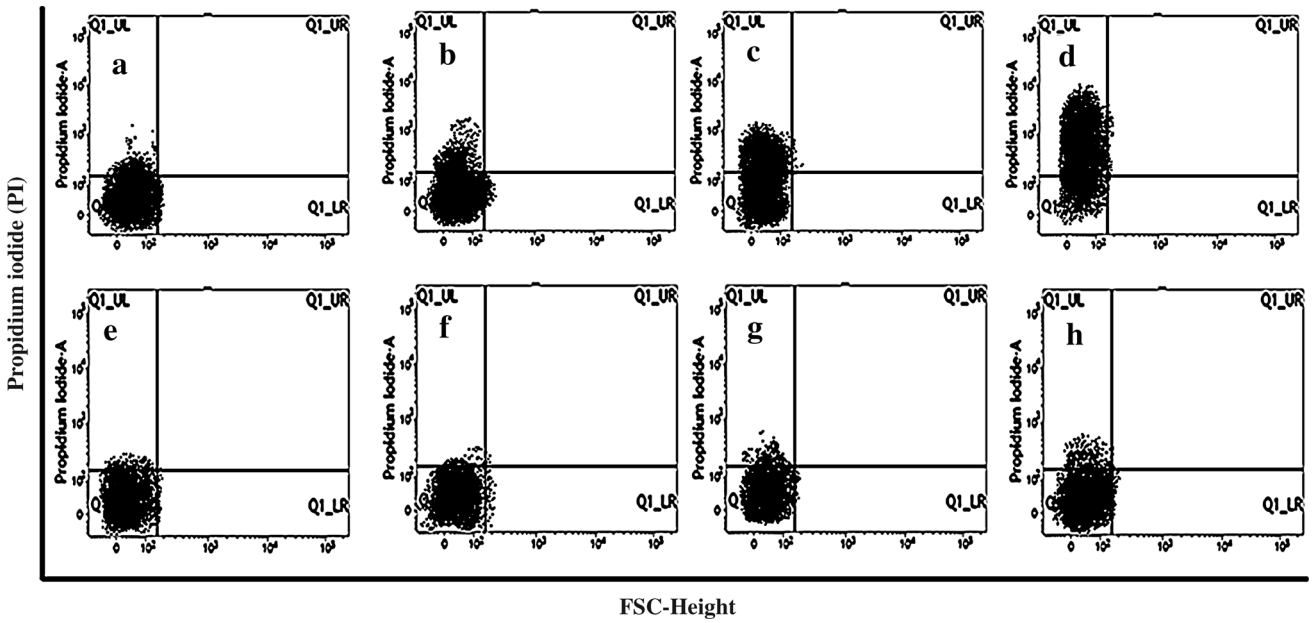

Fig. 7 Flow-cytometric analysis using propidium iodide (*PI*) of cellular apoptosis induced in Jurkat cells by CS-CoO NPs. For each set of samples we used 2×10^4cells per milliliter for analysis of PI-positive cell populations. *a* control, *b* Jurkat cells plus 50 μg/mL CS-CoO NPs, *c* Jurkat cells plus 100 μg/mL CS-CoO NPs, *d* Jurkat cells plus 200 μg/mL CS-CoO NPs, *e* lymphocyte control, *f* lymphocytes plus 50 μg/mL CS-CoO NPs, *g* lymphocytes plus 100 μg/mL CS-CoO NPs, *h* lymphocytes plus 200 μg/mL CS-CoO NPs. *FSC* forward scatter

(Fig. 8a), it is likely that Jurkat cells produced TNF-α in response to CS-CoO NP exposure. The level of the anti-inflammatory cytokine IL-10 is reduced 1.48-fold and 1.01-fold in Jurkat cells at 50 and 100 μg/mL CS-CoO NPs (Fig. 8a). CS-CoO NPs induce proinflammatory cytokines in parallel with the reduction of the levels the anti-inflammatory cytokines. Nanomaterials have been shown to modulate expression of cytokines, which are soluble biological protein messengers that regulate the immune system. Published studies have demonstrated the ability of certain nanomaterials to induce cytokine production, although this appears heavily dependent on a variety of factors, including material composition, size, and method of delivery [44]. Much remains to be learned, however, regarding the proinflammatory potential of CS-CoO NPs. Studies were performed to evaluate the ability of CS-CoO NPs to modulate TNF-α production in primary human immune cells. These particular cytokines were chosen because they represent critical pathways involved in the inflammatory response and differentiation processes. The results demonstrate significant dose-dependent increases in the level of TNF-α at all CS-CoO NP concentrations tested. These results suggest that a synergistic relationship between CS-CoO NPs and TNF-α may occur in in vitro settings using CS-CoO NPs, and demonstrate that CS-CoO NPs are capable of inducing at least some key components of inflammation. The ability of CS-CoO NPs to induce proinflammatory cytokine expression in human primary immune cells is consistent with the recognized relationship between oxidative stress and inflammation, which is partially mediated by induction of the transcription factor NF-κB [45]. CS-CoO NPs induce high levels of TNF-α and help to promote T helper cell type 1 (T_h1) differentiation [46–48] as well as functioning as a regulator of acute inflammation [48]. The ability of CS-CoO NPs to induce TNF-α at concentrations below those that cause appreciable cytotoxicity indicates immunomodulatory effects that may function to bias the immune response toward T_h1-mediated immunity. It is the cytokine profile that directs the development and differentiation of T helper cells into the two different subsets, T_h1 and T helper cell type 2 (T_h2) [45, 49]. Relevant to our findings, TNF-α plays critical roles in T_h1 development, and helps set up a perpetuating loop whereby more T_h1 development is favored and T_h2 development is suppressed by low amounts of IL-10. Thus, our findings indicate that careful titration of CS-CoO NP based therapeutic interventions may be successful in elevating the levels of a group of cytokines important for eliciting a T_h1-mediated immune response with effective anticancer actions. However, high-level and/or long-term exposure to TNF-α has been shown to produce serious detrimental effects on the host, including septic shock or symptoms associated with autoimmune disease [48]. Our results demonstrate significant dose-dependent increases in the level of TNF-α over a somewhat narrow range of CS-CoO NP concentrations. The magnitude of TNF-α induction and that of other proinflammatory cytokines and their local regional delivery to tumor sites or

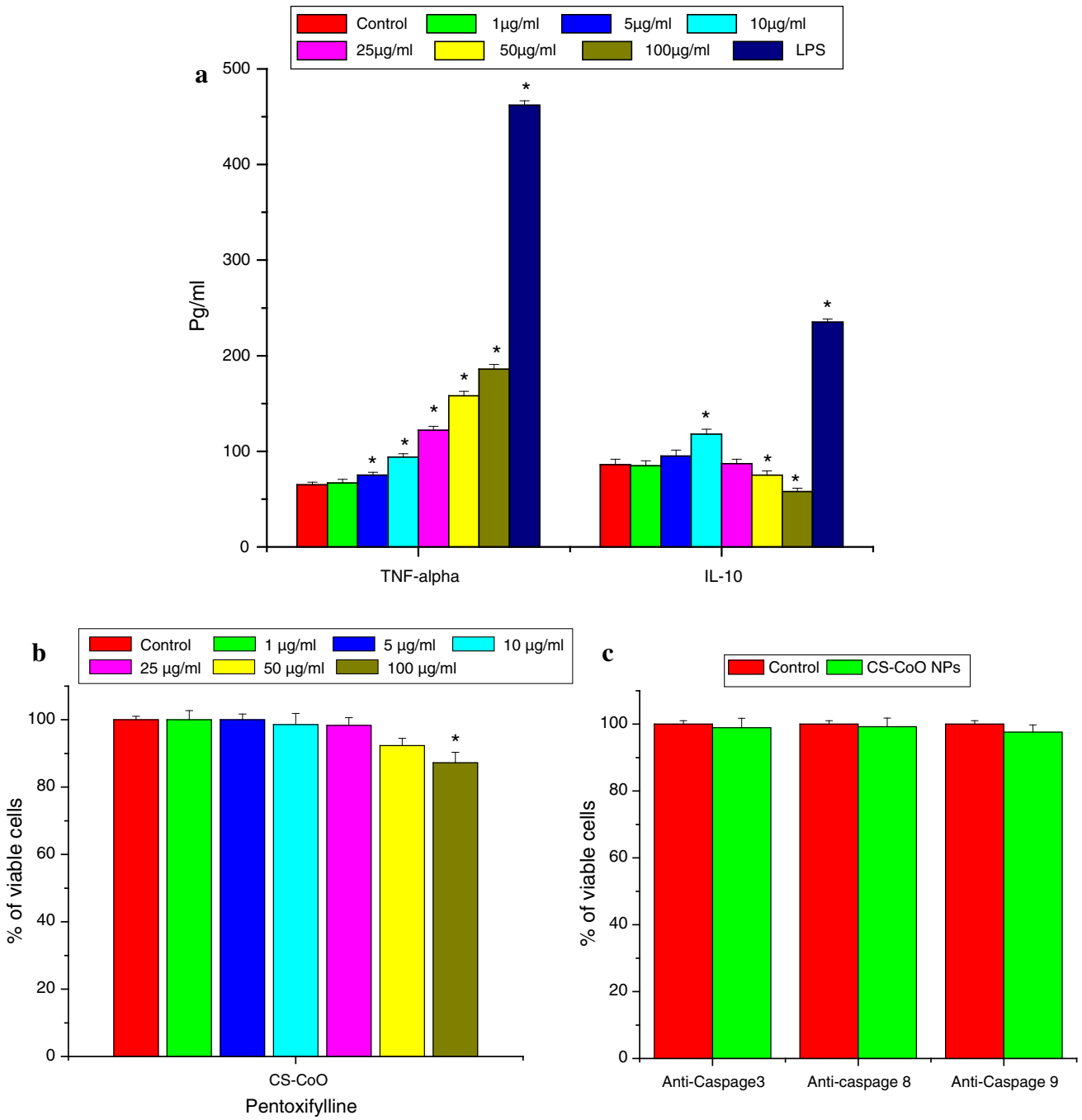

Fig. 8 **a** Proinflammatory and anti-inflammatory effects of CS-CoO NPs on Jurkat cells with regard to TNF-α and IL-10 ($n = 6$; values are expressed as the mean ± SEM). An *asterisk* indicates a significant difference as compared with the control group. **b** Cytotoxicity of CS-CoO NPs toward human lymphoma cells with pentoxifylline at 2 mM and **c** incubation with anti-caspase antibody (caspases 3, 8, 9), with cell viability being measured by the 3-(4,5-dimethyl-2-thiazolyl)-2,5-diphenyl-2*H*-tetrazolium bromide assay ($n = 6$; values are expressed as the mean ± SEM). An *asterisk* indicates a significant difference as compared with the control group

other desired areas will undoubtedly be important parameters when considering CS-CoO NPs for biomedical purposes to achieve the desired therapeutic response without eliciting potential systemic damaging effects from these cytokines.

Inhibition of TNF-α by pentoxifylline

Pentoxifylline and theophylline, both phosphodiesterase inhibitors, have the ability to suppress monocyte/macrophage TNF-α production by increasing the intracellular

accumulation of cyclic AMP [50, 51]. Our study shows that the use of pentoxifylline in culture medium increases Jurkat cell viability by 92.33 and 87.24 % in the presence of CS-CoO NPs at 50 and 100 μg/mL, respectively (Fig. 8-b).The Jurkat cell viability was likely unchanged below a CS-CoO NP concentration of 50 μg/mL. It has been proved that in humans pentoxifylline is able to reduce the release of TNF-α by peripheral blood monocytes [52] and inhibit the synthesis of messenger RNA for TNF-α in mouse peritoneal macrophages at the transcriptional level. Our result shows that TNF-α plays a key role in cancer cell killing mediated by CS-CoO NPs.

Involvement of caspase

Apoptosis requires activation of an upstream caspase [53]. To determine whether CS-CoO NPs induce the activation of this caspase, Jurkat cells were treated with 100 μg/mL CS-CoO NPs and anti-caspase antibodies for 24 h, and cell viability was examined. Jurkat cell viability was increased in the presences of anti-caspase antibodies. The results indicated that CS-CoO NPs activated caspases (3, 8, and 9) in Jurkat cells. Caspases play a critical role in regulating many of the morphological and biochemical features of apoptosis. The role of caspase in triggering apoptosis was demonstrated as an apical initiator caspase in receptor- and stress-induced apoptosis [54]. The induction of apoptosis could, in fact, be prevented by treating cells with an inhibitor of caspases 3, 8, and 9 (Fig. 8c), implying a direct relationship between CS-CoO NP mediated caspase activation and apoptosis of Jurkat cells. Higher expression of inflammatory cytokines such as TNF-α is an established stimulator of the caspase pathway [16, 17]. The present study shows that the use pentoxifylline in culture medium increases Jurkat cell viability (Fig. 8b). Our result clearly demonstrates that inhibition of TNF-α increases cancer cell viability. TNF-α-induced caspase activation is critically involved in apoptosis. Stimulation of cells with CS-CoO NPs was sufficient to induce TNF-α. On binding to TNF receptor 1, TNF-α is able to induce apoptosis through activation of caspase 8 [17]. Our findings are in concurrence with the effect of CS-CoO NPs on Jurkat cells with increasing TNF-α expression and their induction of TNF-α-mediated cell death.

Conclusion

CS-CoO NPs are nontoxic to normal cells up to 100 μg/mL, but in contrast, Jurkat cell viability is reduced significantly at the same dose and above. The intracellular pH is responsible for nanocomplex-mediated Jurkat cell toxicity. CS-CoO NPs stimulate the production of ROS and TNF-α, and these two apoptotic stimuli could induce cell death. A substantial percentage of TNF-α activity characterizes the contribution of the different caspase activation pathways.

Acknowledgments The authors express gratefulness to the Department of Biotechnology, Government of India, for funding. The authors also express gratefulness to the Indian Institute of Technology, Kharagpur, and Vidyasagar University, Midnapore, for providing the facilities to execute these studies.

Conflict of interest The authors declare that they have no conflicts of interest.

References

1. Papis E, Rossi F, Raspanti M, Isabella DD, Colombo G, Milzani A, Bernardini G, Gornati R (2009) Toxicol Lett 189:253–259
2. Parkes LM, Hodgson R, Lu LT, Tung LD, Robinson I, Fernig DG, Thanh NT (2008) Contrast Media Mol Imag 3:150–156
3. Pardoe H, Chua-anusorn W, Pierre TG, Dobson J (2001) J Magn Magn Mater 225:41–46
4. Hubert PM, Guerrero G, Vioux A (2005) J Mater Chem 15:3761–3768
5. Chung YC, Tsai CF, Li CF (2006) Fish Sci 72:1096–1103
6. Shi SF, Jia JF, Guo XK, Zhao YP, Chen DS, Guo YY, Cheng T, Zhang XL (2012) Int J Nanomed 7:5593–5602
7. Chattopadhyay S, Chakraborty SP, Laha D, Baral R, Pramanik P, Roy S (2012) Cancer Nanotechnol 3:13–23
8. Ghosh T, Chattopadhyay T, Das S, Mondal S, Suresh E, Zangrando E, Das D (2011) Cryst Growth Des 11:3198–3205
9. Ma R, Levard C, Marinakos SM, Cheng Y, Liu J, Michel F, Brown GE, Lowry GV (2012) Environ Sci Technol 46:752–759
10. Hudson L, Hay FC (1991) Practical immunology, 3rd edn. Blackwell, Oxford, pp 21–22
11. Chattopadhyay S, Dash SK, Ghosh T, Das D, Pramanik P, Roy S (2013) Cancer Nanotechnol 4:103–116
12. Lin YS, Haynes LC (2010) J Am Chem Soc 132:4834–4842
13. Gaither LA, Eide DJ (2001) J Biol Chem 276(25):22258–22264
14. Hanley C, Layne J, Punnoose A, Reddy KM, Coombs I, Coombs A, Feris K, Wingett D (2008) Nanotechnology 19:295103
15. Roa W, Xiaojing Z, Guo L, Shaw A, Hu X, Xiong Y, Gulavita S, Patel S, Sun X, Chen J, Moor R, Xing JZ (2009) Nanotechnology 20:1–9
16. Wang L, Du F, Wang X (2008) Cell 133:693–703
17. Pelagi M, Curnis F, Colombo B, Rovere P, Sacchi A, Manfredi AA, Corti A (2000) Eur Cytokine Netw 11:580–588
18. Huh PW, Kotasek D, Jacob HS, Vercellotti GM, Hammerschmidt DE (1985) Clin Res 33:866–878
19. Schade UF (1989) Eicosanoids 2:183–187
20. Schade UF (1990) Circ Shock 31:171–181
21. Marques LJ, Zheng L, Poulakis N, Guzman J, Costabel U (1999) Am J Respir Crit Care Med 159:508–511
22. Okada M, Sagawa T, Tominaga A, Kodama T, Hitsumoto Y (1996) Immunology 89:158–164
23. Lowry OH, Rosebrough NJ, Farr AL, Randall RJ (1951) J Biol Chem 193:265–275
24. Das M, Mishra D, Maiti TK, Basak A, Pramanik P (2008) Nanotechnology 19:415101
25. Greish YE, Brown PW (2001) Biomaterials 22:807–816
26. Peer D, Karp JM, Hong S, Farokhzad OC, Margalit R, Langer R (2007) Nat Nanotechnol 2:751
27. Sanpui P, Chattopadhyay A, Ghosh SS (2011) ACS Appl Mater Interfaces 3:218–228

28. Xia T, Kovochich M, Liong M, Ma L, Gilbert B, Shi H, Yeh JI, Jeffrey I, Andre E (2008) ACS Nanotechnol 2(10):2121–2134
29. Gojova A, Guo B, Kota RS, Rutledge JC, Kennedy IM, Barakat AI (2007) Environ Health Perspect 155:403–409
30. Mohapatra S, Mallick SK, Maiti TK, Ghosh SK, Pramanik P (2007) Nanotechnology 18:385102–385111
31. Lovric J, Cho SJ, Winnik FM, Maysinger D (2005) Chem Biol 12:1227–1234
32. Resnitzky P, Bustan A, Peled A, Marikovsky Y (1988) Leuk Res 12:315–320
33. Bergelson LD, Dyatlovitskaya EV, Sorokina IV, Gorkova IB (1974) Biochim Biophys Acta 360:361–365
34. Burlakova EB, Palmina NP, Maltseva EL (1991) In: Vigo-Pelfrey C (ed) Membrane lipid oxidation III. CRC, Boca Raton, pp 209–237
35. Coleman R, Finean JB (1968) Comp Biochem 23:99–126
36. Xia T, Kovochich M, Brant J, Hotze M, Sempf J, Oberley T, Sioutas C, Yeh JI, Wiesner MR, Nel AE (2006) Nano Lett 6:1794–1807
37. Long TC, Saleh N, Tilton RD, Lowry GV, Veronesi B (2006) Environ Sci Technol 40:4346–4352
38. Ryter SW, Kim HP, Hoetzel A, Park JW, Nakahira K, Wang X, Choi AM (2007) Antioxid Redox Signal 9:49–89
39. Carmody RJ, Cotter TG (2001) Redox Rep 6:77–90
40. Yang MH, Jiang JH, Yang YH, Chen XH, Shen GL, Yu RQ (2006) Biosens Bioelectron 21:1791–1797
41. Boudreau RT, Conrad DM, Hoskin DW (2007) Exp Mol Pathol 83:347–356
42. Gupta AK, Gupta M (2005) Biomaterials 26:3992–4021
43. Ishikawa K, Ishii H, Saito T (2006) DNA Cell Biol 25:406–411
44. Federico A, Morgillo F, Tuccillo C, Ciardiello F, Loguercio C (2007) Int J Cancer 121:2381
45. Lappin MB, Campbell JD (2000) Blood Rev 14:228
46. Dong C, Flavell RA (2001) Curr Opin Hematol 8:47
47. Croft M (2009) Nat Rev Immunol 9:271
48. Fishman MA, Perelson AS (1999) Bull Math Biol 61:403
49. Endres S, Fulle HJ, Sincha B, Stoll D, Dinarello CA, Gerzer R, Weber PC (1991) Immunology 72:56–60
50. Spatafora M, Chiappara G, Merendino AM, D'Amico D, Bellia V, Bonsignore G (1994) Eur Respir J 7:223–228
51. Neuner P, Klosner G, Schauer E, Pourmojib M, Macheiner W, Grünwald C, Knobler R, Schwarz A, Luger TA, Schwarz T (1994) Immunology 83:262–267
52. Weber CK, Liptay S, Wirth T, Adler G, Schmid RM (2000) Gastroenterology 119:1209–1218
53. Ashkenazi A, Dixit VM (1998) Science 281(5381):1305–1308
54. Lombaert N, De Boeck M, Decordier I, Cundari E, Lison D, Kirsch-Volders M (2004) Toxicol Lett 154:23–34